

## Noise reduction in TEM: Presenting a bandwidth- and sensitivity-optimized parallel recording setup and methods for adaptive synchronous detection

Nicklas Skovgaard Nyboe<sup>1</sup> and Kurt Sørensen<sup>1</sup>

### ABSTRACT

The transient electromagnetic method (TEM) is a recognized tool for determining the subsurface resistivity structure over a wide depth interval. A key requirement for an accurate characterization of the shallow part of this interval is a sufficiently wideband receiver system. The maximum depth of investigation, on the other hand, is determined by the late-time signal-to-noise ratio (S/N). It has been demonstrated that the use of compact wideband receiver coils tends to deteriorate the late-time S/N due to their inherent low sensitivity to time-varying magnetic fields. To overcome this problem, we used a bandwidth- and sensitivity-optimized parallel recording setup using two separated receiver coils optimized for measuring the early- and late-time part of the transient signal, respectively. Using this setup, we experienced substantial improvements in

the achievable depth of investigation while retaining shallow resolution. Further noise reduction may be obtained by adapting the applied synchronous detection measuring scheme to the local noise conditions. This is especially important when TEM are carried out in culturally developed areas, which is often the case for environmental investigations. Such soundings frequently suffer from inferior signal quality due to EM noise from local cultural sources. Comparing the frequency-domain filtering effect of the applied synchronous detection measuring scheme with the actual noise frequency content allowed us to evaluate the relative importance of the many sources of noise encountered in the field. Further improvements could be obtained by tailoring the applied synchronous detection to better reject specific noise frequencies through modification of the properties of time-gate integration and gate stacking.

### INTRODUCTION

During the past decade, the Department of Earth Sciences of Aarhus University has made significant efforts at developing transient electromagnetic (TEM) instrumentation. This ongoing research was initiated in relation to the large-scale National Groundwater Mapping Program in Denmark — a program which has been going on for the better part of a decade, involving more than 70,000 ground-based TEM soundings (Møller et al., 2009) and roughly 50,000 line-km of airborne TEM (V. H. Søndergaard, personal communication, 2011). Much progress has been achieved in terms of instrument development, data handling, inversion procedures, and dissemination of expertise throughout the involved academic and administrative institutions. Due to the nationwide scale of the investigation, it has been essential to develop instrumentation

providing high fieldwork efficiency without compromising data quality. For ground-based TEM systems, this implies that the equipment must be easy to mobilize when carried manually by a measuring crew typically consisting of only two persons. The depth of investigation extends from the surface down to more than 300 m in typical Danish environments (Jørgensen et al., 2003). Traditional ground-based equipment using  $40 \times 40\text{-m}^2$  transmitter loops cannot achieve such high depths of penetration in routine application (Sørensen et al., 2005). It is well known that the depth of investigation can be increased by applying a higher transmitter moment (Spies, 1989). Common practice is to use a fixed sounding configuration transmitting a low and a high current to resolve early and late time decays, respectively. The achievable transmitter moment then only depends on the magnitude of the transmitter current, which is limited by the restrictions on weight and bulk of the

Manuscript received by the Editor 8 July 2011; revised manuscript received 8 December 2011; published online 20 April 2012.

<sup>1</sup>Aarhus University, Department of Earth Sciences, Aarhus, Denmark. E-mail: nicklas.nyboe@geo.au.dk; kurt.sorensen@geo.au.dk.  
©2012 Society of Exploration Geophysicists. All rights reserved.

transmitter, allowing for easy portability. An appealing alternative approach to increasing the depth of investigation is to reduce the effective noise, thereby increasing the signal-to-noise ratio (S/N). Unfortunately, the methods for achieving this are less obvious. To complement the ongoing instrument development, our research has focused on techniques aiming to reduce the effective noise in near-surface TEM applications.

Air-core induction coils are generally used as sensors of time-varying magnetic fields for the transient method. The sensitivity of an induction coil is directly proportional to its area-turns product, which is a highly unfavorable property for the small, compact receiver coils often used to achieve the high bandwidth necessary for undistorted measurements of early decay times (e.g., PROTEM by GEONICS, SIROTEM by Geo Instruments, TerraTEM by Alpha Geoscience, and NanoTEM by Zonge). In the following sections, we demonstrate how our experiences with small induction-coil receivers in Denmark have revealed that noise inherent to the receiver coil and its preamplifier often constitutes the main contribution to the overall noise measured with this type of TEM instrumentation. Flexible large-area air-core coils, compact ferrite-core coils, and superconducting quantum interference device (SQUID) magnetometers can all achieve higher sensitivity and reduce internal noise compared to compact air-core coils. However, they all suffer from other undesirable properties. As will be described in the section covering induction-coil properties, increasing the induction-coil area introduces difficulties in achieving proper shielding and, more importantly, it reduces the bandwidth of the induction coil. Ferrite-core coils are inappropriate for near-surface TEM application due to distributed, nonnegligible eddy currents induced in the core material during the current turnoff. These eddy currents have large time constants, resulting in a significant bias response at late times (Townsend, 2002). SQUID magnetometers adapted for ground-based TEM measurements represent an interesting and novel approach. Preliminary results indicate impressive noise characteristics, especially at low frequencies where induction-coil sensitivity is inherently low (Foley et al., 1999; Chwala et al., 2001). SQUID magnetometers are, however, significantly more complicated to operate in the field and thus require further development to be implemented in routine measuring situations. Consequently, we consider the air-core induction coil to be the preferred receiver for routine near-surface TEM measurements. To overcome instrument noise as a limiting factor, a bandwidth- and sensitivity-optimized parallel recording setup using two separated induction-coil receivers is proposed. One receiver is a compact, shielded broadband receiver measuring the early time segment of the transient decay; the second is a shielded, flexible receiver with a large area measuring the late-time segment of the transient decay. Consequently, the setup has gained the shorthand title “the segmented receiver setup,” which will be used in the remainder of the paper. A similar TEM measuring setup using two receivers has been outlined briefly by Qian (1985); as of yet, no experiments have been reported. Our experiences with the segmented receiver setup demonstrate astounding improvements in S/N (Nyboe et al., 2010), although the noise-reduction capability exhibits significant temporal and spatial variation. The varying performance is a consequence of varying ambient noise conditions, which primarily affect the effective noise distorting the signal from the larger receiver. Using a sufficiently sensitive receiver, the sensitivity of a TEM system to ambient noise is predominantly determined by the filtering effect of the synchronous detection scheme

applied to the measured signal. Macnae et al. (1984) demonstrate how the filtering properties of synchronous detection can be tailored to better reject certain noise frequencies by applying a linear tapered stacking scheme. With modern digital equipment, the traditional boxcar gate integration can likewise be modified into a smooth gate shape to reduce the influence of high-frequency noise. Furthermore, application of an even smoother tapering of the stacking scheme allows for more efficient suppression of, e.g., electric power transmission noise harmonics of slightly varying frequency. Consequently, a well-designed synchronous detection scheme is paramount to maximize the effectiveness of the proposed segmented receiver setup.

## NOISE IN TEM

The depth of investigation achievable for an impulse-response TEM system using an induction-coil receiver has been shown by Spies (1989) to depend on the effective noise level  $\eta_v$  in  $V/m^2$ , subsurface conductivity  $\sigma$ , and transmitter magnetic moment  $I \cdot A$  as

$$d = 0.55 \left( \frac{IA}{\sigma \eta_v} \right)^{1/5}. \quad (1)$$

The sources contributing to the effective noise level are numerous, and many authors have dealt with the subject of identifying and describing these sources and their impact on TEM measurements (e.g., Macnae et al., 1984; McCracken et al., 1986; Szarka, 1988; Spies and Frichknecht, 1991). Although we will not restate the details here, it should be mentioned that noise affecting TEM measurements is generated by either external or internal sources relative to the instrument. The ambient electric and magnetic fields generated by external sources are of cultural as well as natural origin, whereas the internal sources comprise the noise inherent to the design of the instrument's electronics. Near-surface TEM signals are exceedingly wideband and typically necessitate a system bandwidth ranging from DC to several hundred kilohertz. The naturally occurring electromagnetic (EM) noise in this frequency range is primarily sferics, which emanate from regions of lightning storm activity around the world and propagate with low attenuation in the earth-ionosphere waveguide. Cultural EM noise in the same frequency range is generated by a multitude of sources; for the most part, electrical power transmission and radio communication are the dominant contributors in Denmark. Regarding instrument-generated noise, the general assumption among instrument developers is that it is no longer an issue in TEM measurements because modern instrument design using low-noise components has reduced the influence well below the expected ambient-noise influence. When dealing with compact wideband receiver coils, this assumption appears ill-founded.

We have investigated the prevailing noise conditions in rural and industrial areas in Denmark using various induction-coil receivers. The ambient noise has been monitored at three locations (see Figure 1), and typical time series have been chosen for spectral analysis. Focusing primarily on the noise expected to affect late-time decays, we show the frequency interval from 0 to 30 kHz. Figure 1a presents the noise conditions measured in a remote clearing in a small forest south of Aarhus. Sferics are responsible for the observed noise base level from approximately 3 kHz and upward, whereas VLF transmissions containing significant signal energy

stand out clearly in the 15–30-kHz band. Figure 1b presents the noise conditions measured at the Danish National Test Site for TEM instruments, which is approximately 500 m from a highway encircling Aarhus. Again, a noise base level due to sferics is recognized. Although the high-frequency part of the spectrum is dominated by very-low-frequency (VLF) transmissions, the low-frequency part is dominated by the base 50-Hz and higher harmonics of the electric power transmission noise. Figure 1c presents the noise conditions measured on a field close to an industrial area in Beder, south of Aarhus. Here, the 50-Hz noise and higher harmonics are entirely dominating with VLF transmitters still present. Numerous spurious frequency components are observed, which we expect to be related to nearby heavy industrial activity.

### THE INDUCTION-COIL RECEIVER

The voltage induced in an ideal air-core induction coil due to a time-varying magnetic field is given as (Tumanski, 2007)

$$V(t) = -\mu_0 \cdot A \cdot n \cdot \frac{\partial H}{\partial t}. \quad (2)$$

The induced voltage is proportional to the area-turns product,  $A \cdot n$ , of the coil as well as the time rate of change of the magnetic field. However, this relation is complicated by the finite bandwidth of the actual coil, essentially acting as a second-order oscillatory RLC circuit (Frischknecht, 1987). Consequently, an undamped induction coil has a primary resonance frequency  $f_0$  given by the expression (Tumanski, 2007)

$$f_0 = \frac{1}{2\pi \cdot \sqrt{L \cdot C}}, \quad (3)$$

where  $L$  is the self-inductance of the coil and  $C$  is the parasitic capacitance. Induction coils used for transient measurements typically are critically damped or slightly underdamped to minimize oscillations in the impulse response while maintaining the widest possible frequency band of constant gain (Frischknecht, 1987). As a result, the bandwidth of a properly damped receiver coil is closely related to its undamped resonance frequency. The coil sensitivity can be increased by increasing the area-turns product, although this approach tends to increase the self-inductance of the coil, as expressed by the following empirical, approximate relation (Grover, 1946):

$$L = N^2 \cdot a \cdot \left( 0.6 + 0.8 \cdot \ln \left[ \frac{a}{b} \right] \right). \quad (4)$$

The coil is a square with  $N$  turns, side length  $a$ , and height  $b$  (for length input in meters, the resulting self-inductance is in  $\mu\text{H}$ ). Because the self-inductance increases almost linearly with the length and quadratically with the number of turns, increasing the area-turns product of an induction coil will reduce its bandwidth drastically. It is well known that insufficient receiver-coil bandwidth may produce considerable early time signal distortion, which results in erroneous interpretations if not taken into account (see Effersø et al., 1999). Incorporating the amplitude and phase characteristics of the receiver coil into the inversion algorithm requires substantial knowledge of the receiver-coil parameters and confidence in their stability despite the changing conditions encountered in the field. Low-pass filtering

below the coil cutoff frequency reduces this problem; it is used in most TEM instruments to stabilize the overall system bandwidth and ensure that the phase and amplitude distortion of frequency components near the upper bandwidth limit is well determined. Another major concern in designing the receiver coils is the electrical shielding. An unshielded coil will couple capacitively to the conducting earth surface, affecting the total parasitic capacitance of the coil and, hence, its resonance frequency. The contribution from the capacitance between the earth's surface and the coil in general cannot be predicted because it is highly dependent on the material properties and geometry of the earth's surface in the immediate vicinity of the coil. Furthermore, an unshielded induction coil will act as an E-field antenna, being sensitive to E-field components in the plane of the coil (Ott, 1988). Both effects can be suppressed, if proper electrical shielding is applied, without affecting the sensitivity of the coil to magnetic flux changes (Ott, 1988). Such shielding can be readily achieved for compact and rigid coil geometries, although many years of working with experimental coil design have shown that larger flexible coils are significantly more challenging to shield properly.

A typical TEM recording setup is outlined in Figure 2, specifically indicating the main electrical components constituting a receiver coil. These components are all sources of instrument noise because the coil wire and the damping resistor generate thermal noise, whereas the preamplifier and the signal conditioning

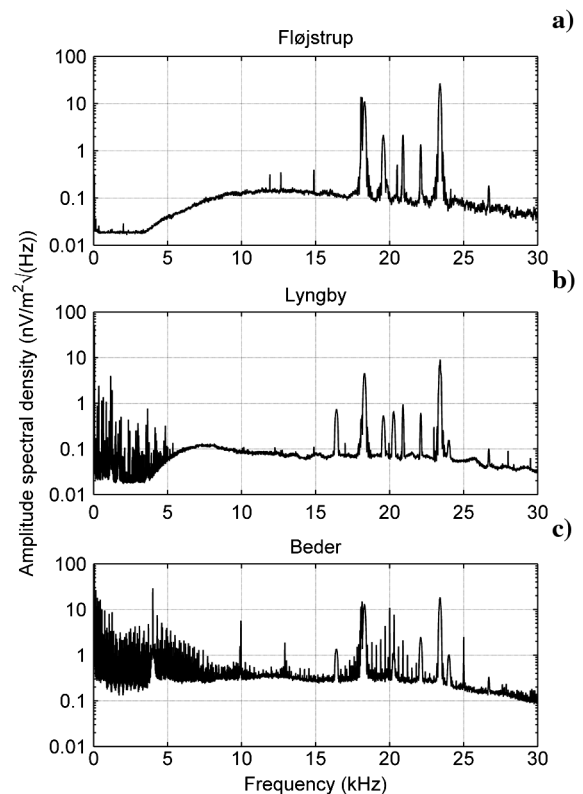


Figure 1. Amplitude spectra of the vertical noise component measured at three locations near Aarhus, Denmark. The length of the corresponding time series is 30 s. They were measured using a 200-m<sup>2</sup> induction coil connected to a 32-kHz second-order antialias filter. Measurements were made in late May and early June under typical Danish summer conditions.

generate a device-specific noise contribution. The combined noise generated by the receiver-coil components is amplified by the (usually high) gain factor of the preamplifier. Due to this amplification, the instrument noise of the receiver coil tends to dominate the subsequent noise contributions along the transmission path as well as in the signal-conditioning and recording steps. Thermal noise exhibits a constant-amplitude spectral density over all frequencies, but preamplifier noise has a constant spectral density over most of its bandwidth, exhibiting  $1/f$  behavior at very low frequencies. Due to the limited amount of wire used in winding compact wideband induction-coil receivers and the low resistance of the damping resistor, the preamplifier noise contribution tends to dominate the thermal noise contribution.

A theory for optimizing receiver sensitivity, according to prevailing levels of ambient EM noise in TEM measurements, is presented by McCracken et al. (1984). The noise problem considered by McCracken et al. is significantly simplified by assuming a constant noise spectral density for natural noise and instrument noise over the bandwidth of interest while ignoring potential influences from cultural noise sources. The bandwidth of interest is much narrower for the treated measuring system than is the case for typical near-surface measuring systems, so the conditions assumed in the paper are seldom encountered in reality for near-surface TEM measurements. It is, nonetheless, notable that the area-turns product necessary for an in-loop receiver coil to be measuring efficiently at high latitudes during high-noise summer conditions is estimated to

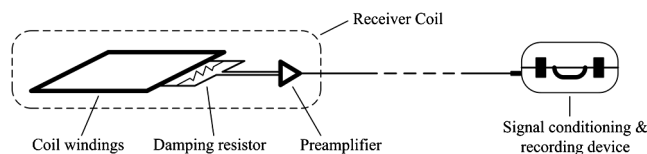


Figure 2. Sketch of the components constituting a typical TEM receiver system.

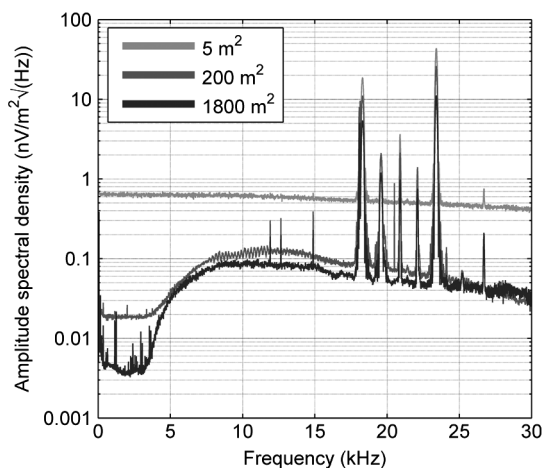


Figure 3. Amplitude spectra of the vertical noise component measured at a single location in Figure 1a using different receiver-coil areas. The length of the corresponding time series is 30 s. All receivers were connected to a 32-kHz second-order antialias filter. The gentle sloping of the 5-m<sup>2</sup> noise level is due to this filter.

exceed 170 m<sup>2</sup>. This area-turns product ensures that the natural noise contribution is of the same magnitude as the instrument noise for the receiver electronics available at the time. In low-noise winter conditions, at high latitudes, this area-turns product must be further increased to an impressive 1700 m<sup>2</sup>.

It is clear that the coil properties such as effective bandwidth, sensitivity to time-varying ambient magnetic fields, internal noise sources, electrical shielding, weight, and size must inevitably be prioritized when designing an induction-coil receiver. The design settled upon for the locally developed wideband receiver coil used extensively in Denmark is a rigid, 0.5 × 0.5 m<sup>2</sup>, 20-turn differential-mode air-core coil having an area-turns product of 5 m<sup>2</sup>. The preamplifier is mounted directly on the coil to minimize the path of unamplified signal transmission. This is important because the unamplified signal is much more susceptible to the influence of external noise sources. The coil is shielded using a cover of semi-conducting material, and state-of-the-art low-noise electronic design and components are applied (Analog Devices R&D department, personal communication, 2011). Still, a noise floor due to instrument noise is clearly visible in the amplitude spectral density plot in Figure 3, displaying ambient noise measured with different induction coils in a remote forest clearing near Fløjstrup, south of Aarhus. This noise floor masks all except the highest spectral noise peaks, indicating that instrument noise may constitute a significant portion of the overall measured noise for compact wideband induction coils. In fact, instrument noise often turns out to be the most important noise source affecting late-time gates when the full filtering effect of synchronous detection is taken into account. This is mainly due to the significant low-pass filtering effect imposed by the wide (a few milliseconds) late-time gates combined with the relatively small flux changes generated by low-frequency ambient magnetic fields.

## SYNCHRONOUS DETECTION

Synchronous detection in TEM is the combined process of signal integration in time gates and subsequent averaging of the integrated time gates from successive measurements of alternating polarity synchronous with the transmitter-current alternations (Becker and Cheng, 1987). Synchronous detection is generally known to be effective in removing slowly varying instrument offset voltages and power-line noise, yet its usefulness stretches much further. Several authors have dealt with the details of the noise-suppressing properties of synchronous detection (San Filippo and Hohmann, 1983; Macnae et al., 1984; Becker and Cheng, 1987) because these properties are crucial for evaluating the performance of a TEM system in the presence of a multitude of noise sources. Notably, Macnae et al. (1984) clarify that a periodic measuring process is indeed localizable in the frequency domain for uncorrelated noise input and that the noise-suppressing effects of synchronous detection can therefore be understood by considering it conceptually as a linear filtering operation. They introduce the concept of a gate-specific filter impulse response called the instrument sampling function  $S(t)$ . An instrument sampling function consists of a reference waveform  $R(t)$  and a weighting function  $W(t)$  related through the equation (Macnae et al., 1984)

$$S(t) = R(t) \cdot W(t), \quad (5)$$

where  $R(t)$  determines the shape, width, and positioning of the sign-alternating and periodically repeating gate windows and  $W(t)$

determines the amplitude of the individual gate windows and thereby the effective averaging time. The sampling function is used to extract an average gate value  $G_{\text{avg}}$  from a time series  $\text{TEM}(t)$ , composed of continuously repeating and sign-alternating earth responses superimposed by additive noise. This gate value is achieved through a convolution operation evaluated at a specific displacement  $\tau_0$ , where  $\tau_0$  is determined by the desired gate center time:

$$G_{\text{avg}} = (\text{TEM}(t) * S(t))|_{t=\tau_0} = \int_{-\infty}^{\infty} \text{TEM}(t) \cdot S(\tau_0 - t) dt. \quad (6)$$

The resulting average gate value is distorted by noise that introduces uncertainty in the estimation. The gate-value variance can be predicted, using standard linear filter techniques, under the assumption that the noise corrupting the periodic TEM signal is sufficiently stationary and uncorrelated with the TEM signal. The magnitude of the synchronous-detection filter frequency response is referred to as the noise spectral sensitivity  $\bar{K}(f)$ , which is the norm of the Fourier transform of  $S(t)$ . Denoting the single-sided noise power spectrum  $|\bar{n}(f)|^2$ , the expected variance of the average gate value is calculated by the relation (Macnae et al., 1984)

$$\sigma_{G_{\text{avg}}}^2 = \bar{K}^2(f) |\bar{n}(f)|^2 df. \quad (7)$$

Equation 7 reveals the possibility of identifying exactly which noise sources need consideration and which can be ignored, given their spectral properties relative to the filtering property of the synchronous detection measuring scheme. Furthermore, it reveals how to optimize the applied synchronous detection to the prevailing noise conditions, which corresponds to modifying the functions  $W(t)$  and  $R(t)$  to tailor their frequency-domain properties to better reject certain noise frequencies. Fourier-series theory dictates that an infinitely repeating periodic signal in time has an amplitude spectrum consisting of discrete spectral lines located at multiples of the base repetition frequency of the signal. Due to the sign-alternating character of the repeating TEM signal, its amplitude spectrum consists of spectral lines only at the base frequency and odd harmonics. The noise spectral sensitivity reflects this behavior by peaking only at these spectral lines and decaying away from them. The noise spectral sensitivity function can, however, be further tailored with respect to two main properties: one is the overall low-pass filtering effect due to the signal integration performed within each gate window, and the other is the shape and width of the peaks as well as the rate of decay away from the peaks. The second property is determined entirely by the shape and width of the weighting function. Macnae et al. (1984) advocate the use of a tapered weighting function and present the advantages of a linear taper relative to uniform weighting. The linear taper does, however, have suboptimal side-lobe suppression due to its discontinuous first derivative. Furthermore, there is no discussion of the possibility of shaping the actual reference waveform to enhance the low-pass filtering effect of gate integration. Implementing significant modifications to the instrument sampling functions of an analog recording system is generally a major task, making it unsuitable for quick adaptation to local noise conditions.

However, the use of digital TEM recording systems, having significant storage capacity, introduces much better options for monitoring noise conditions as well as for modifying the applied system sampling functions in the postprocessing stage to better reject problematic noise frequencies.

In the following, we consider the filtering properties of the two distinct instrument-sampling functions presented in Figure 4. Figure 4a shows the most simple type of sampling function, where the  $R(t)$  function consists of sign-alternating boxcar functions periodically repeating every 40 ms, with each half-period being identical to the one displayed in Figure 4b, and  $W(t)$  is a wide boxcar function bounding an interval containing 64 of the repeating boxcar functions of  $R(t)$ . Figure 4c shows an instrument-sampling function optimized to reject high-frequency noise and narrowband noise between the TEM signal spectral line components. The  $R(t)$  function consists of sign-alternating Gaussian-shaped functions periodically repeating every 40 ms, with each half-period being identical to the one displayed in Figure 4d, and  $W(t)$  is a wide error-function tapered boxcar bounding the same interval as the  $W(t)$  function of Figure 4a. The noise spectral sensitivities of the two instrument-sampling functions are shown in Figure 5, demonstrating the desirable properties of the modified instrument-sampling function. Figure 5a displays the noise spectral sensitivity of the simple instrument-sampling function for low frequencies in a gray nuance and its envelope in black, and Figure 5b magnifies its first spectral peak. Similarly, Figure 5c displays the noise spectral sensitivity of the modified instrument-sampling function for low frequencies; Figure 5d magnifies its first spectral peak. The noise spectral sensitivity of the modified instrument-sampling function enjoys significantly improved overall low-pass filter performance because the Fourier transform of the Gaussian-shaped gate is also Gaussian, which decays rapidly with increasing frequency. The boxcar-shaped gate of the simple instrument-sampling function transforms into a sinc function that decays slowly with frequency, although it contains potentially useful zeroes at certain frequencies. The

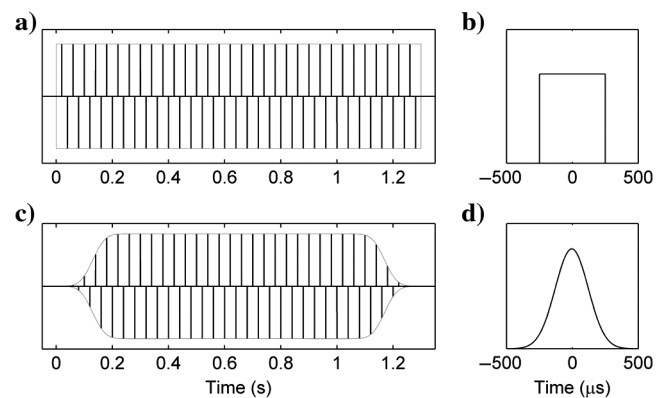


Figure 4. (a, c) Plot of two distinct types of instrument sampling functions, each containing a total of 64 measurements in the stack. The sampling function in (a) represents the simplest type of synchronous detection, which does not include tapering of the stack nor smooth shaping of the gate. The actual gate shape is (b) the 500- $\mu\text{s}$  boxcar function. (c) The sampling function represents a highly adapted type of synchronous detection, with error-function tapering of the stack as well as Gaussian shaping of the individual gates. (d) The Gaussian-shaped gate.

error-function tapered boxcar provides significantly improved side-lobe suppression of the individual peaks compared to the simple boxcar when used as a  $W(t)$  function. Due to the finite duration

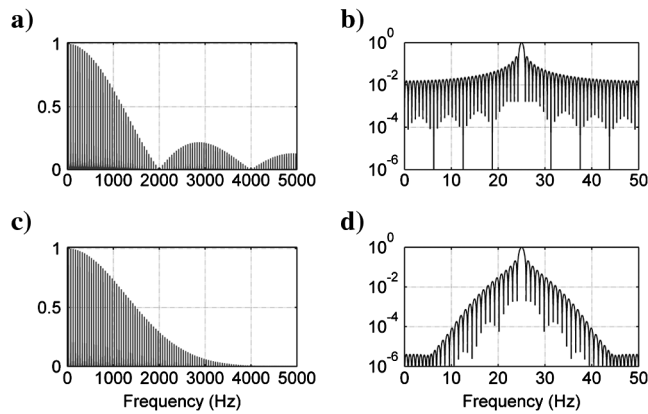


Figure 5. (a, c) The noise spectral sensitivities of the two instrument-sampling functions shown in Figure 4a and 4c. (b, d) Zoomed-in views of the first acceptance peak on a logarithmic vertical scale. These demonstrate the significant reduction in side-lobe amplitude and slight main-lobe widening caused by error-function tapering.

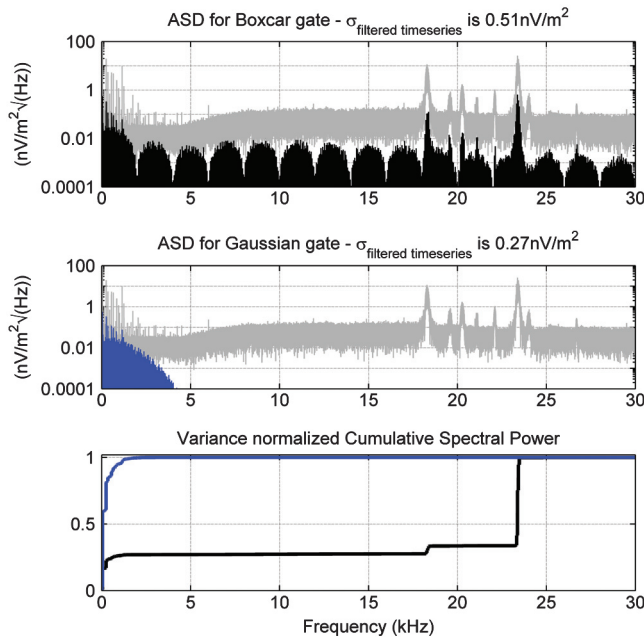


Figure 6. The filtering effect of synchronous detection evaluated on measured noise data through time-domain convolution with the desired instrument sampling function (edge effects removed). The top panel shows the ASD of the measured noise in gray and that of the filtered noise in black. The filtered noise is the result of the measured noise being convolved by the sampling function in Figure 4a. The middle panel displays the same gray spectrum as the top panel; the blue ASD of filtered noise is the result of the measured noise being convolved by a sampling function consisting of a simple boxcar weighting function and Gaussian-shaped gates (combination not shown in Figure 4). The bottom panel shows the normalized cumulative integrated noise power of the two filtered noise series.

of a real-world measurement, a smoothly tapered  $W(t)$  function must jump abruptly to zero at its edges, thereby reducing the achievable level of side-lobe suppression. This is demonstrated in Figure 5d, where the asymptotic behavior of the side lobes changes significantly near 5 and 45 Hz. Tapering in general also reduces the effective duration of the measurement it is applied to, which in synchronous detection has the undesirable effect of widening the main lobe of the individual peaks of the noise spectral sensitivity function. The effect is discernible when comparing Figure 5b and Figure 5d, indicating an increased sensitivity to white noise for the modified instrument-sampling function.

### APPLYING THE INSTRUMENT-SAMPLING FUNCTIONS TO MEASURED NOISE

We have analyzed the performance of various instrument-sampling functions by applying them to noise measurements carried out at a number of Danish locations. This analysis is presented for a noise time series measured using a 200-m<sup>2</sup> receiver coil connected to a second-order 32-kHz antialias filter at the Danish National Test Site for TEM instruments. The noise time series were initially sampled at a rate of 400 kHz and subsequently decimated to 100 kHz to allow for convolution in the time domain by an accurate discrete representation of the instrument-sampling function. Sections influenced by edge effects in the filtered result were subsequently discarded. The standard deviation of the resulting filtered time series approximates the expected standard deviation of the average gate value that would be obtained by a TEM instrument measuring with an equivalent synchronous detection scheme. To identify which frequency components in the filtered noise contribute most to the resulting average gate variance, it is useful to complement the traditional amplitude spectral density (ASD) plot with a plot of variance-normalized cumulative spectral power (CSP). The variance-normalized CSP is calculated by the following expression, using the nomenclature of equation 7:

$$\text{nCSP}(f) = \frac{1}{\sigma_{G_{\text{avg}}}^2} \int_0^f \bar{K}^2(\tilde{f}) |\bar{n}(\tilde{f})|^2 d\tilde{f}. \quad (8)$$

Values of  $\text{nCSP}(f)$  range from zero to one and are monotonically increasing.

The first two instrument-sampling functions being applied are the  $S(t)$  function shown in Figure 4a and a similar  $S(t)$  function where the boxcar gates have been replaced by the Gaussian gates of Figure 4d while retaining the boxcar  $W(t)$  function. The results are presented in Figure 6. The top panel displays the ASD of the original noise measurement in gray and the ASD of the first filtered result in black. The sinc character of the  $\bar{K}(f)$  function shown in Figure 5a is evident. The middle panel likewise displays the ASD of the original noise measurement in gray while displaying the ASD of the second filtered result in blue. The effect of changing gate shape is striking, because all high-frequency noise components are removed entirely. The bottom panel displays the  $\text{nCSP}(f)$  for both of the filtered noise time series, highlighting the main frequency components contributing to the average gate variance in the two cases. For the first  $S(t)$  function, the primary contribution originates from the VLF transmitters located near 18 and 23 kHz as well as some low-frequency contributions due to inadequate cancellation of electrical power transmission noise. For the second  $S(t)$

function, there are practically no contributions from noise sources at frequencies higher than 2 kHz, and effectively all contributions are related to inadequate cancellation of electrical power transmission noise. The standard deviation of the filtered time series ( $\sigma_{\text{filtered timeseries}}$ ) is reduced by a factor of nearly two at this location by changing the gate shape.

The final two instrument-sampling functions being applied employ the Gaussian gates in Figure 4d, while using either the boxcar  $W(t)$  function of Figure 4a or the error function tapered  $W(t)$  function of Figure 4c. The results are presented in Figure 7. The top panel displays a zoomed-in view of the ASD of the original noise measurement in gray and the ASD of the first filtered result in blue. The theoretical zeroing of the 50 Hz and its harmonics, implied by the  $\bar{K}(f)$  function presented in Figure 5b, is clearly not resulting in sufficient suppression of the electrical power transmission noise located at these frequencies. The reason is most likely the electrical power transmission noise not being perfectly stable at 50 Hz and harmonics. The middle panel likewise displays a zoomed-in view of the ASD of the original noise measurement in gray while displaying the ASD of the second filtered result in magenta. The use of a tapered  $W(t)$  function removes all the electrical power transmission noise components due to the significant side-lobe suppression of the  $\bar{K}(f)$  function presented in Figure 5d. Once again, the bottom panel displays the nCSP( $f$ ) for both of the filtered noise time series. For the first  $S(t)$  function, the primary noise contributions originate solely from the base 50 Hz and odd harmonics. For the second  $S(t)$  function, there are no contributions from the electrical power transmission noise, and merely noise at the  $\bar{K}(f)$  peaks contributes to the average gate variance. As demonstrated in Figure 3, the noise floor visible at approximately  $0.02 \frac{\text{nV}}{\text{m}^2 \sqrt{\text{Hz}}}$  in the gray ASD plots is predominantly instrument noise, which indicates that an even larger receiver coil is required to get the full benefits of the modified instrument sampling function. The standard deviation of the filtered time series is reduced further by more than a factor of two at this location by tapering the weighting function. In total, a reduction in standard deviation exceeding a factor of four is achieved by changing from the basic  $S(t)$  function in Figure 4a to the modified  $S(t)$  function in Figure 4c.

We have performed the same analysis for noise measurements carried out using the locally developed 5-m<sup>2</sup> wideband coil, connected to a second-order 32-kHz antialias filter, in identical noise conditions. The analysis revealed that the basic  $S(t)$  function is preferable for this type of receiver due to its superior white-noise-suppressing properties. Referring to Figure 3, this result is a consequence of the instrument-generated white noise dominating most of the considered frequency band. Convolution of the noise measurement with the basic  $S(t)$  function results in a filtered time series having a standard deviation of approximately 2.6 nV/m<sup>2</sup> for the 5-m<sup>2</sup> wideband coil. According to Figures 6 and 7, the standard deviation of the filtered time series for the 200-m<sup>2</sup> coil ranges from 0.51 to 0.11 nV/m<sup>2</sup>, depending on which sampling function is applied. Relative to the 5-m<sup>2</sup> coil, this is a reduction in standard deviation ranging from an approximate factor of 5 to 24. Considering that this corresponds directly to an improvement in S/N of the same factor for an equivalent TEM instrument setup, it is evident that there is a significant potential for noise reduction in using a larger receiver coil combined with adapting the applied instrument sampling function to the local noise conditions.

## THE SEGMENTED RECEIVER SETUP

The reduced sensitivity of the wideband induction-coil receivers typically applied in near-surface TEM soundings inhibits the achievable depth of investigation. To overcome this limitation, we suggest the deployment of a segmented receiver setup consisting of a highly sensitive yet narrowband induction coil and the traditional, less-sensitive wideband induction-coil, measuring simultaneously. This setup allows the receivers to be optimized to the behavior of the TEM signal at early and late times, respectively. The early time TEM signal changes very rapidly and has high amplitude, which makes it ideal to measure using a wideband receiver because sensitivity is not an issue. The late-time TEM signal varies slowly and has much smaller amplitude, which implies that the signal distortion due to the use of a narrowband receiver is insignificant, but the larger sensitivity of the narrowband receiver increases the obtainable S/N. Effectively, we adapt our measurement instrumentation to the character of the signal. We have developed as a sensitive narrowband receiver a flexible yet shielded differential-mode receiver coil with an area of 200 m<sup>2</sup> when laid out in a 10 × 10-m<sup>2</sup> configuration. The increased area generates an induced voltage that is a factor of 40 larger than that of the traditional 5-m<sup>2</sup> wideband receiver, whereas the instrument noise is essentially unchanged due to the application of identical preamplifier electronics. The actual improvement in S/N experienced using the narrowband receiver relative to the wideband receiver may vary quite

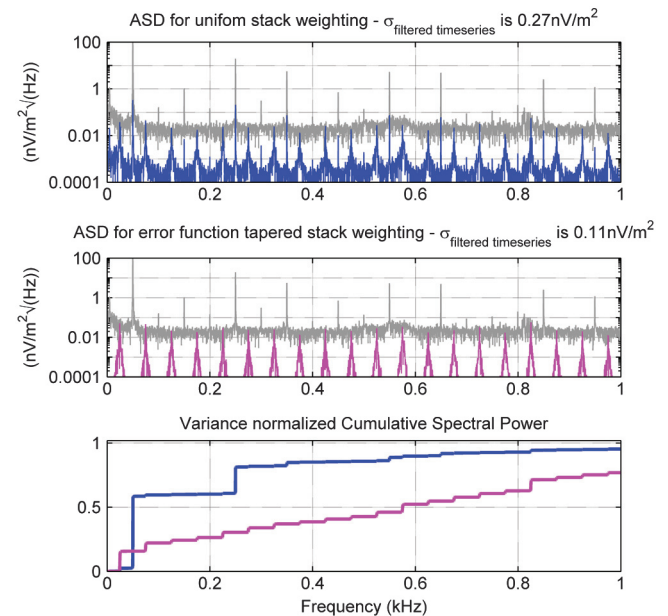


Figure 7. The effect of tapering the stack. The gray curves in the upper and center panels are identical to those of Figure 6 for the presented frequency range. The blue ASD in the top panel is likewise identical to the one in the middle panel of Figure 6 (i.e., no tapering of the stack). The magenta ASD of filtered noise in the middle panel is the result of the measured noise being convolved by the sampling function in Figure 4b, which consists of an error-function tapered stack and Gaussian-shaped gates. The bottom panel displays the normalized cumulative integrated noise power of the two filtered noise series.

substantially because it is highly dependent on local (especially cultural) noise conditions.

We ensure time synchronization between the receiver coils by having two parallel input channels in the data-acquisition box

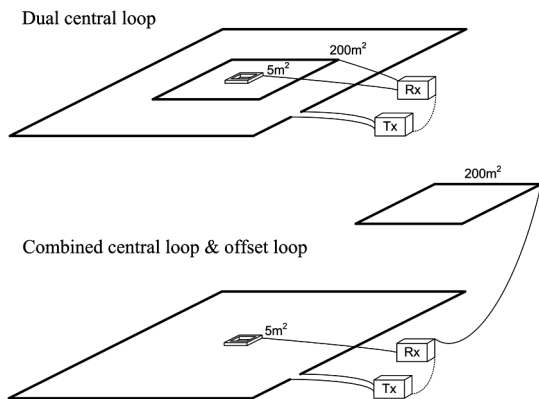


Figure 8. Recommended field layout geometries for the segmented receiver setup.

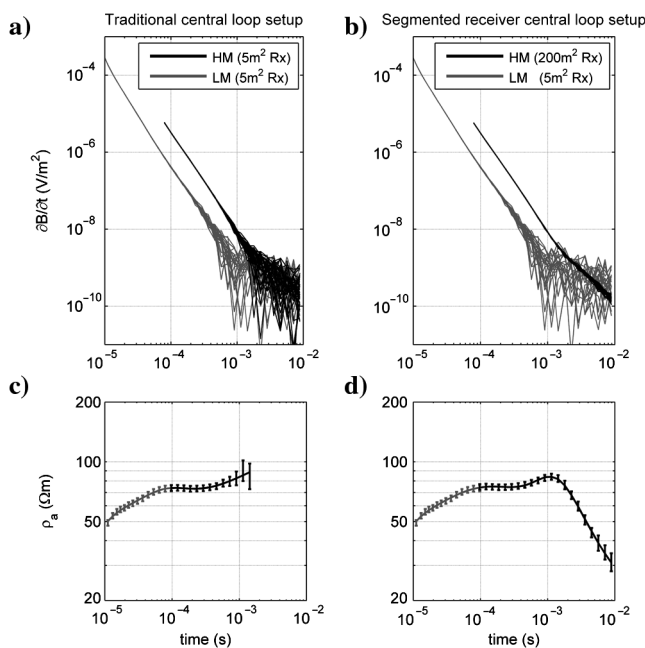


Figure 9. Transient soundings carried out near Rækker Mølle in western Jutland, Denmark. (a) The high- and low-moment measurements resulting from using only the 5-m<sup>2</sup> wideband receiver; (b) the same measurements where the high-moment data are recorded using the 200-m<sup>2</sup> narrowband receiver. Each of the presented  $\partial B/\partial t$  curves represents the average of 1000 single measurements. (c) The  $\rho_a$  transform of the average of the  $\partial B/\partial t$  curves in (a) as uncertainty bars. (d) Similarly, the  $\rho_a$  transform of the average of the  $\partial B/\partial t$  curves in (b) as uncertainty bars. An initial uniform uncertainty of 5% is assumed for the  $\partial B/\partial t$  values, and further uncertainty is assigned based on the calculated standard deviation of the individual gates prior to the  $\rho_a$  transformation. The  $\partial B/\partial t$  values which are assigned a standard deviation exceeding 30% are removed prior to calculating the  $\rho_a$ -transform. The curves intersecting the uncertainty bars in (c) and (d) are the forward-calculated transient responses for the model parameters shown in Table 1.

with a common trigger signal. The coils are calibrated for self-consistency using a two-step process. First, the amplification of the parallel input channels is calibrated in the laboratory using a well-defined input calibration signal. Second, a calibration sounding is performed with the TEM equipment at the Danish National Test Site for TEM instruments. Due to the well-defined geophysical model at the test site, it is possible to produce reliable forward-calculated sounding curves for the applied setup and system parameters. The measured data are compared to the forward-calculated data, allowing the determination of a calibration time shift and shift factor for each coil.

Using two receivers, it is possible to measure with both receivers in a central loop or as a combined central and offset loop setup (see Figure 8). With both receivers in a central loop position, slight signal distortion may occur in the wideband receiver at very early times, when measuring in highly resistive areas, due to mutual inductance between the receiver coils. The combined central and offset loop setup reduces the mutual inductance between receivers and is therefore preferable, despite being slightly more elaborate to set up accurately in a routine measuring situation.

To demonstrate the improvement that can be achieved when applying the segmented receiver setup, a comparison between a traditional TEM sounding and a TEM sounding using the segmented receiver setup is presented in Figure 9a and 9b. The soundings were performed as part of the field campaign reported by Nyboe et al. (2010), who present results obtained using the segmented receiver setup having a 200-m<sup>2</sup> coil as the late-time optimized coil. A number of measurements were carried out in an area in western Jutland, Denmark, with the primary objective of mapping the depth to a conductive formation located at an unknown depth expected to exceed 300 m. The deeply seated conductive formation could not be resolved from data measured using only the traditional wideband receiver coil. However, by applying the segmented receiver setup, it became entirely feasible to map the deeply seated conductive formation at numerous locations without increasing the transmitter magnetic moment while retaining minimal distortion of the early time part of the sounding curve. Concluding the demonstration, the  $\rho_a$ -transformed data presented as uncertainty bars in Figure 9c and 9d have been inverted as four-layer unconstrained 1D models using the software package SiTEM/SEMDI (<http://www.geofysiksamarbejdet.au.dk>). The resulting model parameters and their linearized relative uncertainties are given in Table 1, and the forward-modeled data are shown as curves in Figure 9c and 9d. The relative uncertainties are presented as absolute uncertainties on the logarithm to the model parameters, which represents a good approximation to the actual relative uncertainty for well-determined parameters. The approximation breaks down for poorly determined parameters, but the actual uncertainty of such parameters is not well represented by the linearized posterior covariance matrix in any case. The  $\rho_a$ -transformed data are fitted equally well for both soundings, with the forward curves well within the assigned error bars. The inversion result of the traditional TEM sounding does not indicate a deeply seated conductive layer, but the depth to the top of this layer and its resistivity are very well resolved for the segmented receiver setup TEM sounding.

The presented example clearly demonstrates the improvement in S/N achievable for late-time gates when applying a large receiver coil. It is also demonstrated that the enhanced S/N results in a noticeable increase in resolution for the deeper part of the model.

**Table 1. Results of unconstrained four-layer 1D inversions of the sounding data shown in Figure 9c and 9d.**

Parameter	Traditional central loop setup		Segmented receiver central loop setup	
	Value	Relative uncertainty	Value	Relative uncertainty
Resistivity layer 1	69 $\Omega\text{m}$	0.02	69 $\Omega\text{m}$	0.02
Resistivity layer 2	97 $\Omega\text{m}$	0.41	97 $\Omega\text{m}$	0.53
Resistivity layer 3	42 $\Omega\text{m}$	—	63 $\Omega\text{m}$	0.08
Resistivity layer 4	134 $\Omega\text{m}$	0.41	4 $\Omega\text{m}$	0.26
Thickness layer 1	36 m	0.51	35 m	0.59
Thickness layer 2	53 m	1.64	39 m	1.40
Thickness layer 3	28 m	—	214 m	0.16
Depth to top of layer 2	36 m	0.51	35 m	0.59
Depth to top of layer 3	89 m	0.61	74 m	0.39
Depth to top of layer 4	117 m	0.42	288 m	0.11

A dash indicates a completely undetermined parameter value.

However, the undistorted early time gates can only be obtained when applying the compact wideband receiver coil, which encourages the use of a segmented receiver setup.

### CONCLUSION

We have demonstrated that the instrument noise inherent in compact wideband receiver coils has a significant influence on the depth of investigation achievable when carrying out TEM soundings. Our proposed solution is to simultaneously operate two different receiver coils in a segmented receiver setup, thereby effectively adapting the measurement instrumentation to the character of the transient signal. The usefulness of the segmented receiver setup has been verified at numerous locations, often providing astounding improvements of the S/N.

The actual S/N improvement obtained by applying a second receiver coil depends heavily upon the intensity and character of the ambient noise encountered in the field. The sensitivity of the measurement to the specific ambient noise conditions is essentially determined by the ASD measuring scheme, which acts as a highly frequency-selective filter. For uncorrelated noise sources, the filtering effect is given by the corresponding frequency-domain spectral sensitivity function. We have demonstrated how the spectral sensitivity function can be optimized to better reject specific noise sources through modifications of the gate integration and gate-stacking procedures. Due to temporal and spatial variations in ambient noise characteristics, the improvement in S/N experienced when applying the segmented receiver setup can be enhanced substantially by adapting the synchronous detection-measuring strategy to the local noise conditions.

### ACKNOWLEDGMENTS

We would like to thank the technicians working at the hydrogeophysical workshop at the Department of Earth Sciences at Aarhus University for supporting the ongoing development of TEM instrumentation and for facilitating the practical aspects of the presented research. Likewise, we appreciate Niels Bøie Christensen informally reviewing the paper.

### REFERENCES

- Becker, A., and G. Cheng, 1987, Detection of repetitive electromagnetic signals, *in* M. N. Nabighian, ed., *Electromagnetic methods in applied geophysics: SEG 1*, 443–466.
- Chwala, A., V. Schultze, R. Stolz, J. Ramos, R. IJsselsteijn, H. G. Meyer, and D. Kretzschmar, 2001, An HTS D/C SQUID system in competition with induction coils for TEM applications: *Physica C: Superconductivity and Its Applications*, **354**, 45–48, doi: [10.1016/S0921-4534\(01\)00020-X](https://doi.org/10.1016/S0921-4534(01)00020-X).
- Effersø, F., E. Auken, and K. I. Sørensen, 1999, Inversion of band-limited TEM responses: *Geophysical Prospecting*, **47**, 551–564, doi: [10.1046/j.1365-2478.1999.00135.x](https://doi.org/10.1046/j.1365-2478.1999.00135.x).
- San Filippo, W. A., and G. W. Hohmann, 1983, Computer simulation of low-frequency electromagnetic data acquisition: *Geophysics*, **48**, 1219–1232, doi: [10.1190/1.1441545](https://doi.org/10.1190/1.1441545).
- Foley, C. P., K. E. Leslie, R. Binks, C. Lewis, W. Murray, G. J. Sloggett, S. Lam, B. Sankrithyan, N. Savvides, A. Katzaros, K.-H. Muller, E. E. Mitchell, J. Pollock, J. Lee, D. L. Dart, R. R. Barrow, M. Asten, A. Maddever, G. Panjkovic, M. Downey, C. Hoffman, and R. Turner, 1999, Field trials using HTS SQUID magnetometers for ground-based and airborne geophysical applications: *IEEE Transactions on Applied Superconductivity*, **9**, no. 2, 3786–3792, doi: [10.1109/77.783852](https://doi.org/10.1109/77.783852).
- Frischknecht, F. C., 1987, Electromagnetic physical scale modeling, *in* M. N. Nabighian, ed., *Electromagnetic methods in applied geophysics: SEG 1*, 365–441.
- Grover, F. W., 1946, *Inductance calculations*: Dover Publications Inc., 70–74.
- Jørgensen, F., P. B. E. Sandersen, and E. Auken, 2003, Imaging buried Quaternary valleys using the transient electromagnetic method: *Journal of Applied Geophysics*, **53**, 199–213, doi: [10.1016/j.jappgeo.2003.08.016](https://doi.org/10.1016/j.jappgeo.2003.08.016).
- Macnae, J. C., Y. Lamontagne, and G. F. West, 1984, Noise processing techniques for time-domain EM systems: *Geophysics*, **49**, 934–948, doi: [10.1190/1.1441739](https://doi.org/10.1190/1.1441739).
- McCracken, K. G., M. L. Oristaglio, and G. W. Hohmann, 1986, Minimization of noise in electromagnetic exploration systems: *Geophysics*, **51**, 819–832, doi: [10.1190/1.1442134](https://doi.org/10.1190/1.1442134).
- McCracken, K. G., J. P. Pik, and R. W. Harris, 1984, Noise in EM exploration systems: *Exploration Geophysics*, **15**, 169–174, doi: [10.1071/EG984169](https://doi.org/10.1071/EG984169).
- Møller, I., V. H. Søndergaard, F. Jørgensen, E. Auken, and A. V. Christiansen, 2009, Integrated management and utilization of hydrogeophysical data on a national scale: *Near Surface Geophysics*, **7**, 647–659.
- Nyboe, N. S., F. Jørgensen, and K. Sørensen, 2010, Integrated inversion of TEM and seismic data facilitated by high penetration depths of a segmented receiver setup: *Near Surface Geophysics*, **8**, 467–473.
- Ott, H. W., 1988, *Noise reduction techniques in electronic systems*, 2nd ed.: Wiley.
- Qian, B., 1985, Selection of frequency bandwidth of a TEM receiving system to avoid false anomalies: *Geoexploration; International Journal of Mining and Technical Geophysics and Related Subjects*, **23**, 519–526, doi: [10.1016/0016-7142\(85\)90078-X](https://doi.org/10.1016/0016-7142(85)90078-X).

- Sørensen, K. I., E. Auken, N. B. Christensen, and L. Pellerin, 2005, An integrated approach for hydrogeophysical investigations: New technologies and a case history, *in* D. K. Butler, ed., *Near-surface geophysics*: SEG, 585-605.
- Spies, B. R., 1989, Depth of investigation in electromagnetic sounding methods: *Geophysics*, **54**, 872-888, doi: [10.1190/1.1442716](https://doi.org/10.1190/1.1442716).
- Spies, B. R., and F. C. Frischknecht, 1991, Electromagnetic sounding, *in* M. N. Nabighian, ed., *Electromagnetic methods in applied geophysics*: SEG, 285-426.
- Szarka, L., 1988, Geophysical aspects of man-made electromagnetic noise in the earth — A review: *Surveys in Geophysics*, **9**, 287-318, doi: [10.1007/BF01901627](https://doi.org/10.1007/BF01901627).
- Townsend, J. A., 2002, A comparison of transient electromagnetic sensors for detection of conductive targets beneath conductive overburden: Honors Dissertation, Curtin University Australia, <http://www.geophysics.curtin.edu.au/EGPPUBS/Docs/2002-001355-THN.PDF>, accessed 8 July 2011.
- Tumanski, S., 2007, Induction-coil sensors — A review: *Measurement Science and Technology*, **18**, no. 3, R31-R46, doi: [10.1088/0957-0233/18/3/R01](https://doi.org/10.1088/0957-0233/18/3/R01).